Efficient prestack modeling and imaging of pegleg multiples

Morgan Brown and Antoine Guitton, Stanford University*

SUMMARY

We introduce an efficient linear operator for the "true relative amplitude" modeling and imaging of pegleg multiples. Applying the forward operator to primary reflections after normal moveout models the peglegs. Applying the adjoint operator to multiples produces events which are directly comparable to NMO'ed primaries. The kinematic component of our operator is an extension of the NMO equation which independently images "split" peglegs from a moderately heterogeneous earth. The amplitude component corrects multiples for their differences in angle-dependent reflection strength, relative to a primary. We illustrate the efficacy of our approach on 2D and 3D prestack field data examples.

INTRODUCTION

An important class of multiple suppression methods create a "model" of the multiples, which is subtracted from the data. Most predict multiples from primaries by "adding a multiple bounce" to the data with wavefield extrapolation (Riley and Claerbout, 1976; Morley, 1982; Berryhill and Kim, 1986; Verschuur et al., 1992). Analogous prestack multiple *imaging* methods either explicitly "remove a multiple bounce" from the data, transforming multiples into conventionally imageable pseudo-primary events (Berkhout and Verschuur, 2003; Shan, 2003), or combine the extrapolation and imaging steps (Reiter et al., 1991; Berkhout and Verschuur, 1994; Yu and Schuster, 2001; Guitton, 2002).

Previous authors have cast prestack imaging as an inverse problem with model regularization terms to exploit image multiplicity to fill illumination gaps and increase signal fidelity (Kuehl and Sacchi, 2001; Prucha and Biondi, 2002; Wang et al., 2003). Multiples contain much additional information about the earth's reflectivity, and other works have gone further, presenting inversion methods to jointly image multiples and primaries and combine their information (Brown, 2002; He and Schuster, 2003; Brown, 2004a). The modeling operator in such schemes must be both fast, since it will be applied iteratively (e.g., conjugate gradients), and accurate (kinematics and amplitudes) to avoid biasing the residual error.

We present an efficient prestack modeling/imaging strategy for pegleg multiples, appropriate for both conventional multiple modeling and least-squares joint imaging applications, under the assumption of fairly small reflector dip and lateral velocity variation. The kinematic component of our operator is an extension of the normal moveout (NMO) equation which independently images "split" peglegs from a moderately heterogeneous earth. The amplitude component corrects multiples for their differences in angle-dependent reflection strength, relative to a primary. We illustrate the efficacy of our approach on 2D and 3D prestack field data examples.

KINEMATIC PEGLEG IMAGING IN A 1-D EARTH

In a laterally-homogeneous earth, the NMO equation describes a primary's traveltime at fairly small source-receiver offset:

$$t = \sqrt{\tau + \frac{x^2}{V_{\text{rms}}^2(\tau)}}. \tag{1}$$

Applied as an offset-dependent time shift, equation (1) flattens an arbitrary primary (on a CMP gather) with offset x and root-mean-square (RMS) velocity $V_{\text{rms}}(\tau)$ to its zero-offset traveltime, τ.

Figure 1 motivates an analogous NMO equation for pegleg multiples. Kinematically, a first-order pegleg can be conceptualized as

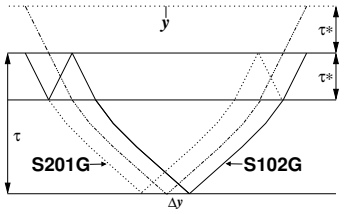

Figure 1: Peglegs "S201G" and "S102G" are kinematically equivalent to "pseudo-primary" with extra zero-offset traveltime τ^*.

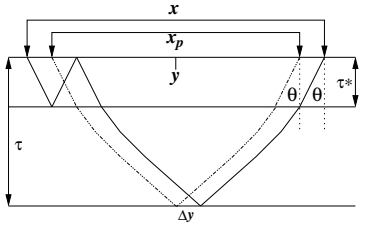

Figure 2: A primary and pegleg multiple with the same emergence angle (θ) and midpoint (y).

a "pseudo-primary" with the same offset, but with an additional two-way zero-offset traveltime to the multiple generator, τ^*. In equation form, let us extend this intuition to the general case of a n^{th}-order pegleg to write an NMO equation for peglegs:

$$t = \sqrt{(\tau + n\tau^*)^2 + \frac{x^2}{V_{\text{eff}}^2}}, \quad \text{where} \tag{2}$$

$$V_{\text{eff}}^2 = \frac{\left(n\tau^* V_{\text{rms}}^2(\tau^*) + \tau V_{\text{rms}}^2(\tau)\right)}{\tau + n\tau^*}. \tag{3}$$

V_{eff}, the pseudo-primary's effective RMS velocity, can be derived directly from the definition of RMS velocity (Brown, 2004b).

AMPLITUDE CORRECTIONS FOR PEGLEGS

Primaries and their multiples recorded at fixed offset traverse different raypaths between source and receiver, and so exhibit different amplitude-versus-offset (AVO) behavior and suffer different anelastic attenuation and geometric spreading losses. In the following sections, we present the Snell Resampling operator to normalize peglegs to their primary with respect to AVO and attenuation, a differential geometric spreading correction for peglegs, and finally, an algorithm to estimate and apply the multiple generator's spatially-variant reflection coeffiecient.

Snell Resampling Normalizes AVO/Attenuation

In a $v(z)$ medium (Figure 2) there exists x_p such that a pegleg with offset x and primary with offset x_p are invariant with respect to AVO and, assuming perfect elasticity above the multiple generator, to attenuation. Noting that the multiple and primary in Figure 2 have the same emergence angle, and thus time dip, at x and x_p, Brown (2004b) obtains:

$$x_p = \frac{x\tau V_{\text{rms}}^2}{\sqrt{(\tau + n\tau^*)^2\, V_{\text{eff}}^4 \;+\; x^2(V_{\text{eff}}^2 - V_{\text{rms}}^2)}} \tag{4}$$

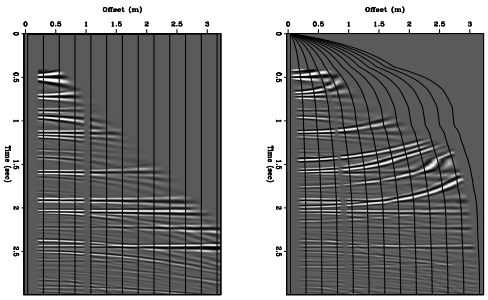

Figure 3: Left: Synthetic CMP gather after NMO. Note two dead and five unrecorded near-offset traces. Right: after NMO for first-order seabed peglegs and (normalized) Snell Resampling.

for a n^{th}-order pegleg. Equation (4) is a compression of the offset axis, which we denote "Snell Resampling". The operator moves multiple energy to its proper location in reflection angle, as shown on Figure 3. The black lines, which depict the offset compression, show how energy from the multiples fills the data's coverage gaps.

The shift, Δy, of the primary and pegleg reflection points (Figure 2) decreases asymptotically to zero from a maximum at the seabed. The actual value depends on the multiple order and reflector depth.

Differential Geometric Spreading
Lu et al. (1999) define offset-dependent geometric spreading corrections for a primary (g_{prim}) and its pegleg multiples (g_{mult}):

$$g_{\text{prim}} = v^* t_{\text{prim}}(x) = \sqrt{(\tau v^*)^2 + \left(\frac{x v^*}{V_{\text{eff}}}\right)^2} \quad (5)$$

$$g_{\text{mult}} = v^* t_{\text{mult}}(x) = \sqrt{[(\tau + n\tau^*)v^*]^2 + \left(\frac{x v^*}{V_{\text{eff}}}\right)^2}, \quad (6)$$

where v^* is the surface velocity. After scaling by $g_{\text{mult}}/g_{\text{prim}}$ and Snell Resampling, we assume that the amplitude of an imaged pegleg and its primary are consistent, to within a reflection coefficient.

Estimation/Application of Seabed Reflection Coefficient
We assume that a multiple generator's reflectivity varies in space, but not in reflection angle. Denote $\mathbf{p}(t,x,y)$ and $\mathbf{m}(t,x,y)$ as small windows in time, offset, and midpoint around a primary and its first pure multiple after normalized Snell Resampling and differential geometric spreading correction. We optimize the reflection coefficient, $\mathbf{r}(y)$, to minimize the following quadratic functional:

$$\sum_{k=1}^{ny}\sum_{j=1}^{nx}\sum_{i=1}^{nt} \mathbf{w}_k^2 \left[\mathbf{r}_k \cdot \mathbf{p}_{i,j,k} - \mathbf{m}_{i,j,k}\right]^2 + \epsilon^2 \sum_{k=2}^{ny} \left[\mathbf{r}_k - \mathbf{r}_{k-1}\right]^2. \quad (7)$$

The second term imposes on $\mathbf{r}(y)$ a degree of smoothness, governed by the tradeoff parameter, ϵ. The optional weight, $\mathbf{w}(y)$, reflects the data's "quality" at y. Using x_p, we can compute the multiple bounce point in a 1D earth for any type of pegleg. A first-order pegleg is scaled by a single reflection coefficient, a second-order pegleg by reflection coefficients from two locations, and so on.

PEGLEG IMAGING IN A HETEROGENEOUS EARTH

An i^{th}-order pegleg (Figure 1) actually consists of $i+1$ unique events. Dipping reflectors cause the events to "split" into individual legs, as Figure 5 shows. Legs with a high apparent velocity hamper Radon demultiple and velocity analysis. Even if reflectors dip only mildly, splitting often causes far-offset tuning effects between the

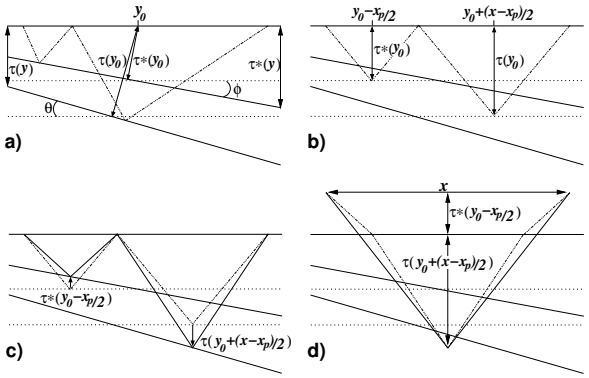

Figure 4: HEMNO schematic. (a): True pegleg raypath. (b): Assumed 1D earth reflection points. (c): Stretch raypath vertically to match measured $\tau^*(y_0 - x_p/2)$ and $\tau(y_0 + (x - x_p)/2)$. Panel (d) Connect legs of raypath; solid line is final result.

legs that can introduce a false multiple AVO signature. To accurately model the kinematics and amplitudes of peglegs, therefore, we must extend the previous 1D theory to handle pegleg splitting.

Levin and Shah (1977) deduced moveout equations for split 2D peglegs, and Ross et al. (1999) extended the work to 3D. Both approaches require constant velocity and locally planar reflectors. To overcome these limitations, we present a model-based imaging method, which we call HEMNO (Heterogeneous Earth Multiple NMO Operator). For small dips, (Brown, 2004b) shows that HEMNO reduces to Levin and Shah's equations.

Figure 4 illustrates HEMNO. Panel a) shows a pegleg raypath with dipping reflectors. Panel b) shows the 1D theory's implied raypath. In Panel c) we account for nonflat reflectors by vertically stretching the 1D raypath to match the zero-offset traveltime at the known 1D reflection points. The stretched raypath disobeys Snell's Law, so in panel d) we connect the tails of the rays to produce a valid raypath with the equation of a hyperbola with offset x and zero-offset traveltime $\tau^*(y_0 - x_p/2) + \tau(y_0 + (x - x_p)/2)$. We first define:

$$\tau_m = \tau^*(y_0 - x_p/2) \qquad \text{and} \qquad \tau_p = \tau(y_0 + (x - x_p)/2), \quad (8)$$

and then write the HEMNO equation directly:

$$t^2 = \left(\tau_m + \tau_p\right)^2 + \frac{x^2}{V_{\text{eff}}^2}. \quad (9)$$

Applying equation (9) as a dynamic time shift flattens the S102G pegleg in offset and shifts the event to the primary's zero-offset traveltime. Similar expressions may be derived for other pegleg types. By using V_{eff}, we ignore lateral velocity variation, consistent with the small dip assumption. Figure 5 shows a split salt-related pegleg, and HEMNO flattens each multiple leg independently.

Implementing equation (9) requires two quantities: τ_m, obtained by hand or auto-picking, and more challengingly, τ_p, an arbitrary reflector's zero-offset traveltime. We obtain τ_p automatically by event tracking, using measured zero-offset reflector dip, which may be estimated automatically (Fomel, 2002), or manually, with picked reflectors and spline interpolation (Brown, 2004b).

Combined imaging/modeling operator
We defined a kinematic multiple modeling/imaging operator and an appropriate suite of amplitude correction operators which now allow us to define a mapping between a prestack image space,

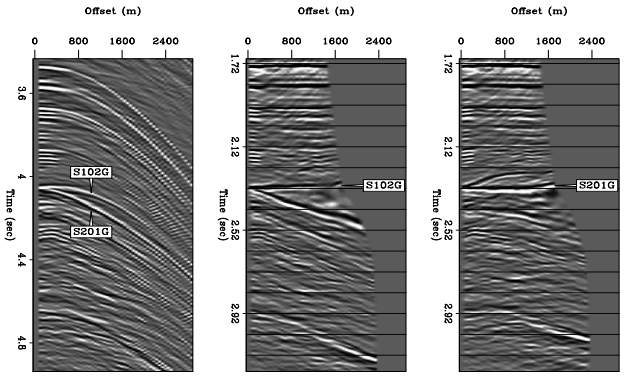

Figure 5: Left: Real CMP gather with split first-order top of salt pegleg (labels indicate the two legs). Pegleg apexes shift away from zero offset. Center and Right: HEMNO (plus previous amplitude corrections) applied to the two legs.

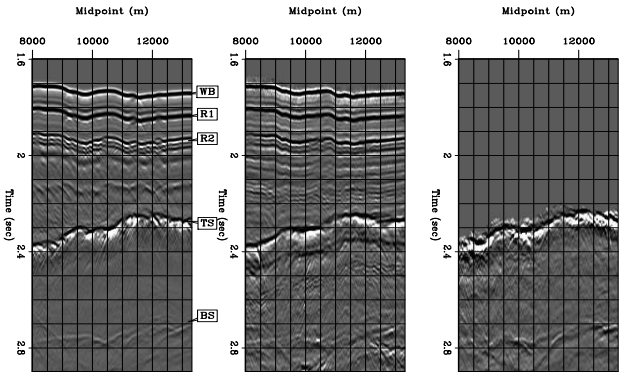

Figure 6: Mississippi Canyon data: imaging and stack. Left: Raw data. Center and right: Seabed (WB) and top of salt (TS) peglegs.

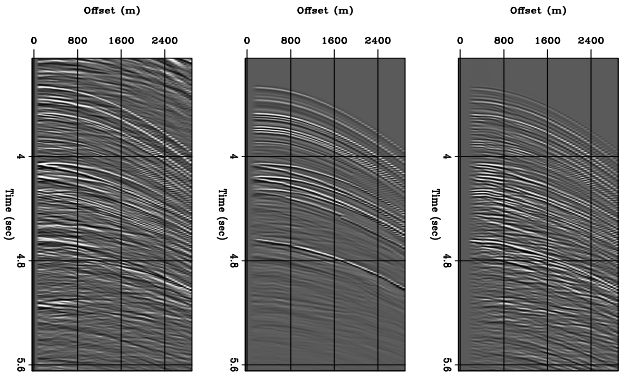

Figure 7: Left: raw CMP gather. Center: HEMNO multiple model. Right: SRME multiple model.

which contains events which resemble imaged primaries, and a data space, which contains events which resemble the recorded pegleg multiples. The image corresponding to the k^{th} leg of the i^{th}-order pegleg from the m^{th} multiple generator, ($\mathbf{m}_{i,k,m}$) is mapped into data space ($\mathbf{d}_{i,k,m}$) by sequentially applying the differential geometric spreading correction ($\mathbf{G}_{i,m}$), Snell Resampling ($\mathbf{S}_{i,m}$), HEMNO ($\mathbf{N}_{i,k,m}$), and finally, the reflection coefficient ($\mathbf{R}_{i,k,m}$):

$$\mathbf{d}_{i,k,m} = \mathbf{R}_{i,k,m}\,\mathbf{N}_{i,k,m}\,\mathbf{S}_{i,m}\,\mathbf{G}_{i,m}\,\mathbf{m}_{i,k,m}\,. \qquad (10)$$

$\mathbf{m}_{i,k,m}$ should resemble flattened primaries. If we have a prior estimate of the primaries, we can use it to create a multiple estimate, $\mathbf{d}_{\text{mult}}$ by summing over all the i, k, and m in equation (10). A crude, but readily available primary estimate comes directly from the recorded data, $\mathbf{d}$, by applying NMO, $\mathbf{N}_0^T$:

$$\mathbf{d}_{\text{mult}} = \sum_{i=1}^{p}\sum_{k=0}^{i}\sum_{m=1}^{n_{\text{surf}}} \mathbf{R}_{i,k,m}\,\mathbf{N}_{i,k,m}\,\mathbf{S}_{i,m}\,\mathbf{G}_{i,m}\,\mathbf{N}_0^T\,\mathbf{d}. \qquad (11)$$

If we set $p = 1$, $\mathbf{d}_{\text{mult}}$'s kinematics are exact (within HEMNO's limitations) only for the predicted first-order multiples. If the estimated primaries contain first-order multiples, equation (11) maps them to events which resemble second-order multiples, but are kinematically inexact. In the subsequent deepwater data examples, second-order multiples can be ignored.

FIELD DATA RESULTS

Figure 6 illustrates our operator's ability to image peglegs on a 2D line from Mississippi Canyon, Gulf of Mexico. The right two panels result from applying the adjoint of equation (10) for peglegs generated by the seabed and top of salt, and then stacking. Notice that the multiple images contain coherent "noise" events not present in the primary image. These "crosstalk" events include peglegs from other multiple generators, primaries, and to a lesser extent, *P*-to-*S* converted waves and interbed multiples. As discussed in detail by Brown (2004a), crosstalk thwarts attempts to integrate information from multiples by simple averaging, and motivates casting joint imaging as an inverse problem to simultaneously separate and combine multiples and primaries.

Given sufficiently dense source and receiver coverage, as with 2D marine data, the autoconvolutional "SRME" (Surface-Related Multiple Elimination) method Verschuur et al. (1992) effectively models surface-related multiples without prior information. Figures 7 and 8 compare multiples modeled by applying one SRME convolution with those modeled by equation (11).

Figure 7 contains many strong multiples from the top of a tabular salt body, including the split peglegs between $\tau = 4.0$ and 4.3 seconds. Both approaches accurately model the multiple splitting. The SRME convolution doubles the near-offset gap, and unless the near-offset traces are pre-interpolated, SRME cannot predict near-offset multiples. Our method images by vertical stretch, and so models near-offset multiples.

Figure 8 compares medium-offset slices taken from the raw data, the SRME multiple model, and our multiple model. Again, we see that both methods do a reasonable job of modeling the split peglegs (circle), although our method sometimes underperforms (tall oval). Again, because SRME is an autoconvolutional method, some wavelet stretch will occur; note a generally lower frequency content in the SRME model.

Figures 9 and 10 illustrate our multiple modeling strategy applied to 3D field data from Green Canyon, Gulf of Mexico. In this (common) acquisition geometry, the crossline offset axis for a given CMP gather has only one live bin, so if we tabulate the live bin's offset value and input it to HEMNO, we can ignore the crossline offset axis (Brown, 2004b) to reduce data volume. HEMNO images by vertical stretch, so it is insensitive to sparse crossline sampling. It images non-flat reflectors using measured zero-offset dip. Figure 9 shows a near-offset section of the data and the predicted multiples (192 by 14 CMP locations). Events are positioned ac-

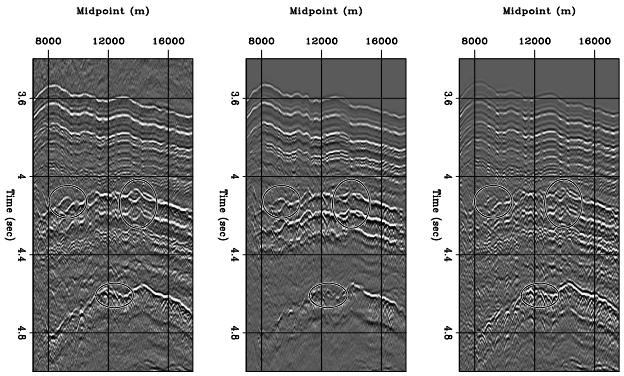

Figure 8: Left: raw medium-offset section. Center: HEMNO multiple model. Right: SRME multiple model.

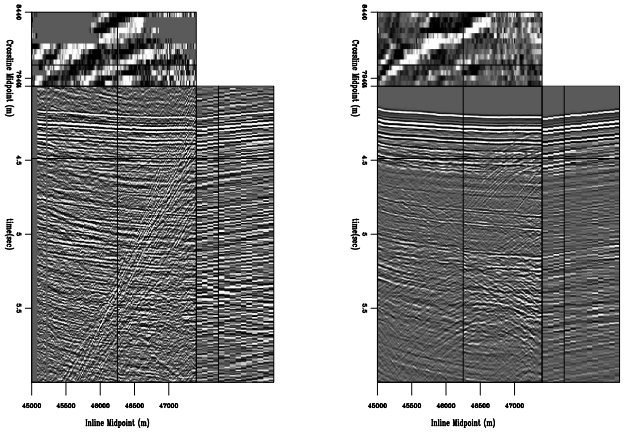

Figure 9: Near-offset section from 3D field data. Left: Raw data. Right: HEMNO multiple model.

curately, in spite of crossline dip that could hamper (2D) SRME. Figure 10 shows one CMP gather of the raw data and the predicted multiples. Fast ship speed led to coarse offset sampling, so many deep events are incoherent, though our approach predicts the strongest multiples.

CONCLUSIONS

We introduced an efficient pegleg multiple imaging/modeling scheme, suitable for joint imaging or multiple suppression applications. On 2D field data, our method predicted multiples that compared favorably to those predicted by SRME. Our method performed well on narrow-azimuth 3D field data with nontrivial crossline dip.

ACKNOWLEDGEMENTS

We acknowledge WesternGeco for donation of the 2D Mississippi Canyon data, and CGG for donation of the 3D Green Canyon data.

REFERENCES

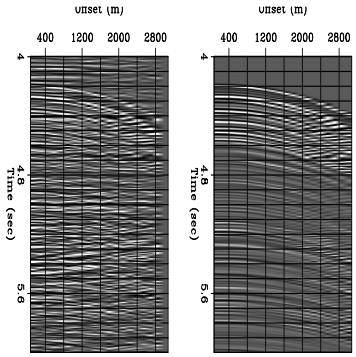

Figure 10: CMP gather from 3D field data. Left: Raw data after NMO. Right: HEMNO multiple model.

Berkhout, A. J., and Verschuur, D. J., 1994, Multiple technology: Part 2, migration of multiple reflections: 64th Ann. Internat. Mtg, 1497–1500.

Berkhout, A. J., and Verschuur, D. J., 2003, Transformation of multiples into primary reflections:, *in* 73rd Ann. Internat. Mtg Soc. of Expl. Geophys.

Berryhill, J. R., and Kim, Y. C., 1986, Deep-water peglegs and multiples - Emulation and suppression: Geophysics, **51**, no. 12, 2177–2184.

Brown, M., 2002, Least-squares joint imaging of primaries and multiples: 72nd Ann. Internat. Mtg, 890–893.

Brown, M., 2004a, Least-squares joint imaging of multiples and primaries: SEG Exp. Abstracts, submitted.

Brown, M. P., 2004b, Least-squares joint imaging of multiples and primaries: Ph.D. thesis, Stanford University.

Fomel, S., 2002, Applications of plane-wave destruction filters: Geophysics, **67**, no. 06, 1946–1960.

Guitton, A., 2002, Shot-profile migration of multiple reflections: 72nd Ann. Internat. Mtg, 1296–1299.

He, R., and Schuster, G., 2003, Least-squares migration of both primaries and multiples:, *in* 73rd Ann. Internat. Mtg Soc. of Expl. Geophys.

Kuehl, H., and Sacchi, M., 2001, Generalized least-squares DSR migration using a common angle imaging condtion: 71st Ann. Internat. Mtg, 1025–1028.

Levin, F. K., and Shah, P. M., 1977, Peg-leg multiples and dipping reflectors: Geophysics, **42**, no. 05, 957–981.

Lu, G., Ursin, B., and Lutro, J., 1999, Model-based removal of water-layer multiple reflections: Geophysics, **64**, no. 6, 1816–1827.

Morley, L., 1982, Predictive multiple suppression: Ph.D. thesis, Stanford University.

Prucha, M. L., and Biondi, B. L., 2002, Subsalt event regularization with steering filters: 72nd Ann. Internat. Mtg., Soc. of Expl. Geophys., Expanded Abstracts, 1176–1179.

Reiter, E. C., Toksoz, M. N., Keho, T. H., and Purdy, G. M., 1991, Imaging with deep-water multiples: Geophysics, **56**, no. 07, 1081–1086.

Riley, D. C., and Claerbout, J. F., 1976, 2-D multiple reflections: Geophysics, **41**, no. 04, 592–620.

Ross, W. S., Yu, Y., and Gasparotto, F. A., 1999, Traveltime prediction and suppression of 3-D multiples: Geophysics, **64**, no. 1, 261–277.

Shan, G., 2003, Source-receiver migration of multiple reflections:, *in* 73rd Ann. Internat. Mtg Soc. of Expl. Geophys.

Verschuur, D. J., Berkhout, A. J., and Wapenaar, C. P. A., 1992, Adaptive surface-related multiple elimination: Geophysics, **57**, no. 09, 1166–1177.

Wang, J., Kuehl, H., and Sacchi, M. D., 2003, Least-squares wave-equation avp imaging of 3D common azimuth data:, *in* 73rd Ann. Internat. Mtg Soc. of Expl. Geophys.

Yu, J., and Schuster, G., 2001, Crosscorrelogram migration of IVSPWD data: 71st Ann. Internat. Mtg, 456–459.